Dynamical optimal positioning of a photovoltaic panel in all weather conditions

Marko Gulin*, Mario Vašak, Nedjeljko Perić

University of Zagreb, Faculty of Electrical Engineering and Computing,
Department of Control and Computer Engineering, Laboratory for Renewable Energy Systems,
Unska 3, 10000 Zagreb, Croatia

Abstract

In this paper we develop and verify a model predictive control algorithm for photovoltaic panel orientation with the aim to maximize the photovoltaic system netto power production. Thereby we take into account local weather forecast with its uncertainty, thermal behavior of the panel, and the positioning system energy consumption with its technical constraints. The model predictive control synthesis procedure comprises two basic steps: (i) identification of solar irradiance model and development of the photovoltaic system model and (ii) development of predictive control algorithm for the photovoltaic panel active surface orientation, based on the obtained models. Performance of the developed algorithm is verified through year-scale simulations based on a large number of solar irradiance and other weather data patterns. It turns out that the proposed algorithm is fully competitive with the mostly used sun tracking or maximum irradiance seeking controls, and that it outperforms them. The other advantages of the proposed algorithm are: (i) the positioning system is controlled smoothly and (ii) prediction of energy yield one day ahead is available together with its uncertainty for easier photovoltaic system integration into the electricity distribution network.

Keywords: Photovoltaic system with dual-axes positioning, Solar radiation modelling, Unscented transformation, Model predictive control, Stochastic optimization

1. Introduction

Importance of renewable energy sources in the world grows rapidly due to the following reasons: (i) renewable sources represent an inexhaustible potential of energy for the future, (ii) price fluctuations and limited resources of fossil fuels that are still dominant in the world's energy sources structure, (iii) the aspiration of national economies towards energy independence, etc. Among renewable sources, solar energy is one of the most promising nowadays [1] and is predicted by numerous analyses to become the mostly used energy resource by 2050 [2].

Stochastic and intermittent nature of the solar energy resource is an aggravating circumstance for the mass use of photovoltaic (PV) systems and their integration into utility grids. PV panels power production mainly depends on the available solar irradiance. The total solar irradiance that reaches the surface of the PV panel in the form of the direct and diffuse irradiance, is influenced by the PV panel active surface orientation. The computation of trajectory for the PV panel active surface orientation (in short: positioning trajectory) throughout a day can be realized in an open-loop or a closed-loop fashion. The open-loop systems pre-compute trajectories for the individual axes positioning systems based on weather forecast data which is refreshed once or several times a day. The closed-loop systems use the information on the current weather conditions (most usually photo sensors) to compute the trajectories.

The authors in [3] proposed closed-loop control system to maximize the solar irradiance incident with the active surface of a PV panel which is necessarily based on the maximum seeking control strategies (perturb and observe principle). Due to the permanent position changes, these systems can spend more energy than they gain, especially when the weather is changing. Many commercial positioning systems are realized as open-loop control systems where they use predefined trajectories for tracking the solar disk position. In this way, most of the direct irradiance is being harvested since rays of the solar disk are perpendicular to the active surface of a PV panel. However, during cloudy conditions when diffuse irradiance prevails, this algorithm does not increase energy output of a PV system. A vast majority of the developed open-loop control systems presumes clear-sky conditions [4, 5]. The authors in [6, 7] proposed advanced open-loop control system, where they use model predictive control for maximizing energy output of a PV system. Because of the simplicity of the used solar irradiance prediction model, proposed method is meant only for clear-sky conditions, and yet in a deterministic framework. Presuming clear-sky conditions is appropriate for climates with a large num-

*Corresponding author. Tel.: +385-1-6129-529; fax: +385-1-6129-809
Email addresses: marko.gulin@fer.hr (Marko Gulin), mario.vasak@fer.hr (Mario Vašak), nedjeljko.peric@fer.hr (Nedjeljko Perić)

ber of sunshine hours, but additional gain is achievable by taking varying weather conditions into account. The authors in [8] proposed that during the clear-sky conditions a PV panel should track the solar disk since direct irradiance prevails, while during the overcast conditions when diffuse irradiance prevails, a PV panel should be placed horizontally, since diffuse irradiance is scattered all over the sky. Although proposed method shows good results, there is no clear algorithmic distinction between clear-sky and overcast conditions.

This paper presents a method for determining the maximum netto energy gain trajectories of the open-loop dual-axes positioning system in a stochastic framework, by considering: (i) local weather forecast and its uncertainty, (ii) solar irradiance model and its uncertainty, (iii) dynamic panel temperature model, and (iv) positioning system energy consumption with its technical constraints. In the used framework of model predictive control this leads to a constrained nonlinear optimization problem, and for solving it an evolutionary algorithm called Differential Evolution (DE) [9, 10] is applied. Data flow diagram of the proposed control algorithm is shown in Figure 1.

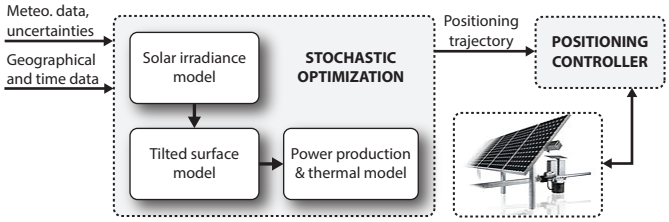

Figure 1: Data flow diagram

The paper is structured as follows. In Section 2 a neural-network-based identification of parametric direct (normal) and diffuse (horizontal) solar irradiance models, along with development of uncertainty of the identified models is described. In Section 3 a PV system model is introduced, considering the uncertainty of available meteorological data and of the developed solar irradiance models. In Section 4 a method for determining the maximum efficiency trajectories of the open-loop dual-axes positioning system, based on DE, is presented. Simulation-based study of the developed algorithm and its comparison with state-of-the-art dual-axes positioning approaches is presented within Section 5.

2. Identification of neural-network-based direct and diffuse solar irradiance models

Knowledge of the local solar irradiance is essential for the proper design of model predictive control algorithm that maximizes the production of electrical power by the PV system. To this aim, a parametric model [11] for site-specific direct (normal) and diffuse (horizontal) solar irradiance as static functions of geographical and meteorological data is developed. For that purpose we use Radial Basis Function (RBF) type neural network [12, 13]. Its training is performed on past geographical and meteorological data and solar irradiance measurements [14, 15] taken from the National Solar Radiation Data Base (NSRDB) for Washington DC Dulles International Airport (WDC Dulles) for period 1996–2003, and its validation is performed for period 2004–2005. Input data used for neural network training are: (i) solar zenith angle, (ii) local air pressure, (iii) dry-bulb temperature, (iv) precipitable water vapor thickness, (v) aerosol optical thickness, (vi) total cloud cover, and (vii) opaque cloud cover.

Solar irradiance data available in NSRDB are in one-hour resolution and represent the energy received per unit area via corresponding irradiance type within the hour-interval that ends at the time-stamp, named solar insolation [16]. This fact must be especially taken care of since our goal is to obtain the static model of the current solar irradiance that takes current geographical and meteorological data as inputs. The RBF network input data is therefore distanced one minute in time, such that linear interpolation of NSRDB full-hour data is used to compute the input meteorological data for the model. The input geographical data for the model (i.e. solar zenith angle) is obtained via known relations for calculating the sky position of the solar disk [17]. The solar irradiance neural network output data are for training reasons integrated on an hour time-scale and compared with NSRDB data. Prior to neural network training process, output data are filtered in order to retain only high-quality direct–diffuse irradiance measurement pairs for identification. For more details on used neural network structure see [18].

2.1. Objective function

The neural network is trained by numerical procedure that tends to minimize the following criterion:

$$\Im \equiv \frac{1}{2}\sum_{i=1}^{N} e^2(\mathbf{X}_i, \mathbf{\Theta}), \tag{1}$$

where $\mathbf{X}$ is the set of NSRDB input data, $\mathbf{\Theta}$ are neural network parameters, N is the number of data $\mathbf{X}_i$ in different time (full-hour) instants and the error e is defined as:

$$e_i \equiv e(\mathbf{X}_i, \mathbf{\Theta}) = I_{NSRDB,i} - \sum_{j=0}^{\tau} [k_j f(\mathbf{X}_{i,j}, \mathbf{\Theta})], \tag{2}$$

where f is the trained solar irradiance function, $I_{NSRDB,i}$ is solar insolation entry in NSRDB for either direct or diffuse solar irradiance, the sum represents a numerical integral of function f within the hour, τ is either 60 or smaller (smaller only for the cases of sunrise and sunset hours), $\mathbf{X}_{i,j}$ are input data within the hour i on the minute resolution – linearly interpolated meteorological data within the hour or the computed instantaneous solar zenith angle, and k_j are numerical integration weights given with:

$$k_j = \begin{cases} \frac{1}{2}\frac{1}{60} & \text{for } j = 0, \tau, \\ \frac{1}{60} & \text{otherwise.} \end{cases} \tag{3}$$

2.2. Identification results

Separate neural networks are trained for the direct and diffuse solar irradiance. Performance measures used for models verification on the validation data set are Mean Bias Error (MBE) and Root Mean Square Error (RMSE):

$$\text{MBE} = \frac{1}{N}\sum_{i=1}^{N} e_i, \quad \text{RMSE} = \sqrt{\frac{1}{N}\sum_{i=1}^{N} e_i^2}. \tag{4}$$

The validation data set consists of the data for WDC Dulles in period 2004–2005. The validation results of the developed models and of the most competitive existing parametric model – METSTAT [19] are presented in Figure 2(a) for the direct (normal) solar irradiance, and in Figure 2(b) for the diffuse (horizontal) solar irradiance models.

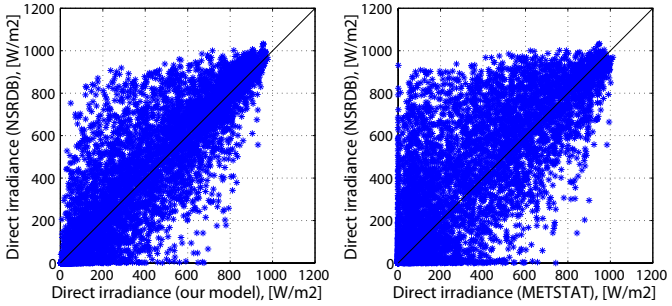

(a) Direct irradiance measurements and model output comparison

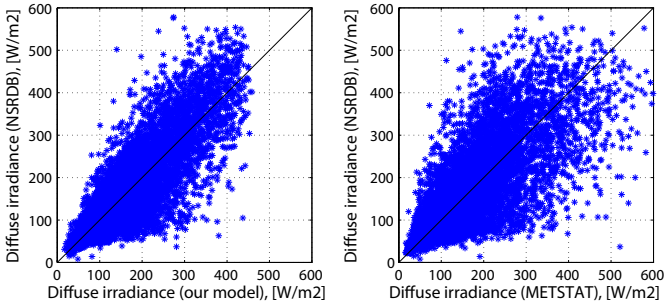

(b) Diffuse irradiance measurements and model output comparison

Figure 2: Solar irradiance measurements and model output comparison

The neural network training is approached by a gradi ent-based Levenberg-Marquardt algorithm [18, 20] and a population-based Particle Swarm Optimization algorithm [21, 22]. Both trainings are performed a large number of times starting from random initial parameters, with exception of Gaussian functions variance [23], and using different hidden layer size, in order to ascertain that the best performing neural network is near the global optimum.

Table 1 shows performance indicators of the developed models and of the METSTAT model on the validation data set. It can be observed that the developed site-specific solar irradiance parametric model realized through RBF neural networks gives significantly better results than a non-site-specific parametric model like METSTAT.

Table 1: Performance measures values (Wm^{-2})

	Direct irradiance		Diffuse irradiance	
	MBE	RMSE	MBE	RMSE
Our model	19.00	157.28	1.00	61.85
METSTAT	59.57	213.60	1.18	82.55

2.3. Uncertainty of the developed models

The developed solar irradiance models are extended with their uncertainty. To this aim, a grid in direct–diffuse irradiance space is formed, with a resolution of 20 Wm^{-2}. Each grid cell contains direct–diffuse irradiance pairs from which bias and variance is calculated.

Cell bias $\mathbf{e}_{bd,i}$ is defined as a vector that contains direct and diffuse irradiance mean errors:

$$\mathbf{e}_{bd,i} = \left[\ \tfrac{1}{m_i}\textstyle\sum_{k=1}^{m_i} e_{b,i,k} \quad \tfrac{1}{m_i}\textstyle\sum_{k=1}^{m_i} e_{d,i,k}\ \right]^\top, \tag{5}$$

where m_i is a number of direct–diffuse irradiance pairs belonging to the ith grid cell, while $e_{b,i,k}$ and $e_{d,i,k}$ are model errors calculated with (2). Covariance matrix $\mathbf{P}_{bd,i}$ of the ith grid cell is defined as:

$$\mathbf{P}_{bd,i} = \frac{1}{m_i}\boldsymbol{\sigma}_i\boldsymbol{\sigma}_i^\top, \tag{6}$$

where deviation $\boldsymbol{\sigma}_i$ is defined as:

$$\boldsymbol{\sigma}_i = \left(\mathbf{y}_{mdl,i} - \mathbf{y}_{meas,i}\right) \ominus \mathbf{e}_{bd,i} = \tilde{\mathbf{e}}_i \ominus \mathbf{e}_{bd,i}, \tag{7}$$

where $\mathbf{y}_{mdl,i}$ and $\mathbf{y}_{meas,i}$ are integrated solar irradiance model output within the hour and measured insolation from NSRDB, respectively, for the entire ith grid cell. In equation (7), operator $\ominus$ is defined as a subtraction of each column of matrix $\tilde{\mathbf{e}}_i$ with column vector $\mathbf{e}_{bd,i}$. Matrix $\tilde{\mathbf{e}}_i$ is of dimension $2 \times m_i$.

Developed solar irradiance models output is in the minute resolution, while measured insolation in NSRDB is in the hour resolution. In order to compare these samples, a numerical integration within the hour is performed. The direct–diffuse samples of a certain hour are placed in the appropriate grid cell based on the minute sample that is in the middle of the analyzed hour.

3. Photovoltaic system model

In this section two models are introduced: (i) a model for solar irradiance incident with a tilted surface and (ii) a PV panel power production and thermal model.

3.1. Solar irradiance incident with a tilted surface

There are many models developed recently [24, 25] used to calculate solar irradiance incident with a tilted surface from known direct (normal) and diffuse (horizontal) solar irradiance components. Main difference between them is in the concept of whether or not the diffuse solar irradiance is isotropically distributed over the sky. The authors

in [26] reported that Klucher's anisotropic model shows the best approximation abilities, and it is thus used here.

The total solar irradiance incident with a tilted surface $I_{t,T}$ comprises three basic components: (i) beam component $I_{b,T}$, (ii) sky diffuse component $I_{d,T}$, and (iii) reflected component $I_{r,T}$:

$$I_{t,T} = I_{b,T} + I_{d,T} + I_{r,T}. \tag{8}$$

Solar irradiance components incident with a tilted surface can be expressed as (Klucher's anisotropic model) [27]:

$$\begin{aligned} I_{b,T} &= I_b \cos\theta, \\ I_{d,T} &= I_d \cos^2\tfrac{\beta}{2}\left[1 + F\sin^3\tfrac{\beta}{2}\right]\left[1 + F\cos^2\theta\sin^3\theta_z\right], \\ I_{r,T} &= \rho(I_b\cos\theta_z + I_d)\sin^2\tfrac{\beta}{2}, \end{aligned} \tag{9}$$

where I_b and I_d are direct (normal) and diffuse (horizontal) solar irradiance components, respectively, θ is the angle between the sun direction and the normal direction of a tilted surface, θ_z is the zenith angle of the sun, β is the tilt angle above horizon of a tilted surface, ρ is the ground albedo and F is a modulating function defined by:

$$F = 1 - \frac{I_d}{I_t}, \tag{10}$$

where I_t is the total solar irradiance incident with a horizontal surface, defined as:

$$I_t = I_b\cos\theta_z + I_d. \tag{11}$$

The angle between the sun direction and the normal direction of a tilted surface, with angles description shown in Figure 3, can be expressed as [28]:

$$\cos\theta = \cos\theta_z\cos\beta + \sin\theta_z\sin\beta\cos(\gamma_s - \gamma), \tag{12}$$

where γ_s and γ are the solar and the PV panel's active surface azimuth angles, respectively.

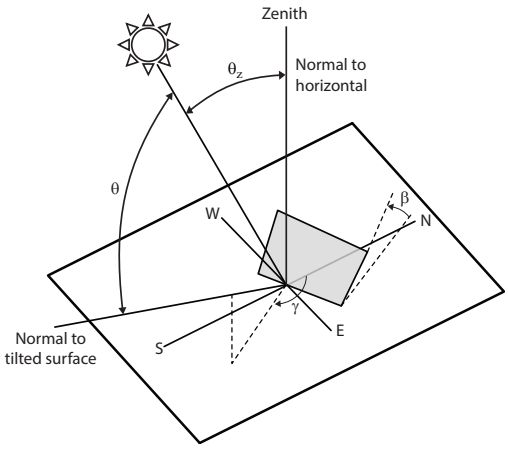

Figure 3: Zenith angle θ_z, angle of incidence θ, tilt angle β and azimuth angle γ for a tilted surface [28]

3.2. *Stochastic characterization of solar irradiance incident with the PV panel active surface*

The Unscented Transformation (UT) is introduced to obtain the statistical description of the overall irradiance on a tilted surface based on the statistical description of input meteorological data and of the developed solar irradiance models. UT is a method for calculating the statistical description of a random variable which undergoes a nonlinear transformation [29].

Consider propagating a random variable $\mathbf{x}$ through a nonlinear function, $\mathbf{y} = f(\mathbf{x})$. Assume $\mathbf{x}$ has mean $\bar{\mathbf{x}}$ and covariance $\mathbf{P_x}$. To calculate the statistics of $\mathbf{y}$, in terms of approximation of its mean $\bar{\mathbf{y}}$ and covariance $\mathbf{P_y}$, a matrix $\boldsymbol{\mathcal{X}}$ of sigma vectors $\boldsymbol{\mathcal{X}}_i$ is formed, according to:

$$\boldsymbol{\mathcal{X}} = \left[\ \bar{\mathbf{x}},\quad \bar{\mathbf{x}} \oplus \alpha\sqrt{\mathbf{P_x}},\quad \bar{\mathbf{x}} \ominus \alpha\sqrt{\mathbf{P_x}}\ \right], \tag{13}$$

where $\oplus$ and $\ominus$ are operators for summation and subtraction of column vector on the left with each column of a matrix on the right, respectively, and α is a weighting factor. The sigma vectors $\boldsymbol{\mathcal{X}}_i$, being the columns of $\boldsymbol{\mathcal{X}}$, are then propagated through the nonlinear function:

$$\boldsymbol{\mathcal{Y}}_i = f(\boldsymbol{\mathcal{X}}_i), \qquad i = 0, \ldots, 2L, \tag{14}$$

where L is the dimension of the input variable $\mathbf{x}$. The mean and the covariance for output $\mathbf{y}$ are approximated using a weighted sample mean and covariance of the posterior sigma points:

$$\bar{\mathbf{y}} \approx \sum_{i=0}^{2L} W_i^{(m)} \boldsymbol{\mathcal{Y}}_i, \tag{15}$$

$$\mathbf{P_y} \approx \sum_{i=0}^{2L} W_i^{(c)} \{\boldsymbol{\mathcal{Y}}_i - \bar{\mathbf{y}}\}\{\boldsymbol{\mathcal{Y}}_i - \bar{\mathbf{y}}\}^\top, \tag{16}$$

where $W_i^{(m)}$ and $W_i^{(c)}$ are weighting factors. UT is selected since it has a superior performance in approximating $\bar{\mathbf{y}}$ and $\mathbf{P_y}$ compared to techniques that reside on pointwise linearization of the nonlinear function f [29].

Figure 4 shows the computation sequence in the stochastic characterization of solar irradiance incident with the PV panel active surface. Input meteorological data with corresponding uncertainty (see Section 2) is represented with sigma vectors as described in equation (13). For each of the 15 obtained sigma vectors, the direct and diffuse solar irradiance is calculated using the developed solar irradiance RBF neural network model.

To take into account the uncertainty of the RBF neural network model itself (see Section 2.3), the obtained set of 15 direct–diffuse solar irradiance pairs is extended with additional pairs, in a way that each of the generated 15 points in $\mathbb{R}^2$ is characterized with sigma vectors that represent the point stochastic description in terms of RBF models uncertainty. They designate the possible locations of the actual direct–diffuse pair when the uncertainties of the input data and the RBF model act simultaneously. The

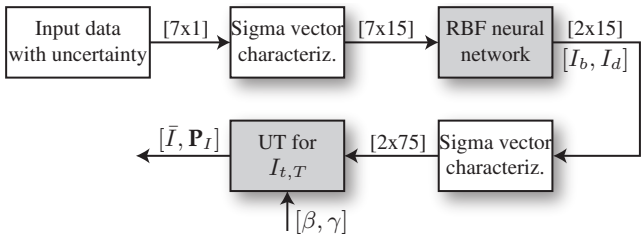

Figure 4: Stochastic characterization computation sequence

UT is then performed on the resulting set of 75 direct–diffuse pairs based on given β and γ, and the result is the stochastic characterization of total solar irradiance incident with the PV panel active surface.

3.3. Power production and thermal model of a PV panel

The PV panel temperature is a function of the weather conditions, the PV panel configuration, the physical parameters of the PV panel material and of the surrounding environment. A simple static model of PV panel cannot provide satisfactory results during periods of fluctuating changes in solar irradiance (i.e. when a cloud suddenly covers the sun) [30] and it is therefore necessary to use a dynamic PV panel thermal model in advanced PV panel positioning control applications.

Panel temperature estimation is based on heat transfer between the PV panel and its environment. All three modes of heat transfer are considered [31]: (i) conduction, (ii) convection, and (iii) radiation. Besides aforementioned heat transfer modes, generated electrical output power is also a form of heat removal. Combining these forms of heat transfers we reach the final mathematical model that describes the thermal dynamics of a PV panel:

$$C_m \frac{dT_m}{dt} = q_{sw} + q_{lw} + q_{conv} - P_{out}, \tag{17}$$

where C_m is the lump heat capacity of the panel, T_m is the panel temperature, q_{sw} and q_{lw} are short- and long-wave radiation, q_{conv} is heat convection, and P_{out} is the PV panel generated electrical power. The PV panel output power is implemented in a form of a 2D array, determined by incident solar irradiance and the PV panel temperature, with a resolution of 1 Wm^{-2} and 1 °C.

4. Model predictive control of orientation of the PV panel active surface

This section describes a method for determining the tilt and azimuth angle trajectories for maximum energy production of the PV system. Thereby the following is considered: (i) local weather forecast and its uncertainty, (ii) solar irradiance model and its uncertainty, (iii) dynamic panel temperature model, and (iv) positioning system energy consumption with its technical constraints.

4.1. The optimization problem

Objective function used in the considered maximization procedure is defined as a netto produced electrical energy of a PV system on a daily sunshine-duration time horizon:

$$\Im \equiv h(\boldsymbol{\beta}, \boldsymbol{\gamma}) = E_{netto} = E_{pv} - E_c, \tag{18}$$

where E_{pv} is the overall produced electrical energy of the PV system on the considered prediction horizon, E_c is energy consumption of the positioning system given in a form of the angle change dependent functions [6, 7], and $\boldsymbol{\beta}$ and $\boldsymbol{\gamma}$ are tilt and azimuth angle time-dependent trajectories, defined as follows:

$$\begin{aligned} \boldsymbol{\beta} &= \begin{bmatrix} \beta_0 & \beta_1 & \dots & \beta_{N-1} \end{bmatrix}^\top, \\ \boldsymbol{\gamma} &= \begin{bmatrix} \gamma_0 & \gamma_1 & \dots & \gamma_{N-1} \end{bmatrix}^\top, \end{aligned} \tag{19}$$

where β_k and γ_k denote constant tilt and azimuth angles on time interval $[kT, kT+T)$, where $k \in \mathbb{Z}$, and T is the time resolution of positioning.

The nonlinear optimization constraints that must be fulfilled are defined as follows:

$$\beta_{min} \leq \boldsymbol{\beta} \leq \beta_{max}, \qquad \boldsymbol{\beta} \in \mathbb{R}^N, \tag{20a}$$
$$\gamma_{min} \leq \boldsymbol{\gamma} \leq \gamma_{max}, \qquad \boldsymbol{\gamma} \in \mathbb{R}^N, \tag{20b}$$
$$\beta_k = m_\beta \beta_q, \qquad m_\beta \in \mathbb{Z}, \tag{20c}$$
$$\gamma_k = m_\gamma \gamma_q, \qquad m_\gamma \in \mathbb{Z}, \tag{20d}$$

where β_{min}, β_{max}, γ_{min} and γ_{max} are minimum and maximum allowed surface tilt and azimuth angles, respectively, β_q and γ_q are the positioning system resolution quants for tilt and azimuth angles, and N is the prediction horizon of the control problem.

Expressions (20a) and (20b) force the trajectories $\boldsymbol{\beta}$ and $\boldsymbol{\gamma}$ to stay inside the range of motion, and expressions (20c) and (20d) represent quantisation effect of the considered positioning system. The constraints are posed solely on the manipulated variables which results in a trivial space of feasible points and facilitates search for the optimum.

The optimization procedure is performed in a stochastic framework, with optimization goal that tends to maximize the expectation of netto produced electrical energy of a PV system:

$$J(\boldsymbol{\beta}, \boldsymbol{\gamma}) = \mathbf{E}\Big\{ E_{netto}\big(\boldsymbol{\beta}, \boldsymbol{\gamma}, \mathbf{M}, \mathbf{G}, \mathbf{C}_0\big) \Big\}, \tag{21}$$

where $\mathbf{E}(\cdot)$ is the expectation of the observed variable, $\mathbf{M}$ and $\mathbf{G}$ are meteorological and geographical data with uncertainties for the sunshine period of the day, and $\mathbf{C}_0$ are initial conditions:

$$\mathbf{C}_0 = \big(\beta_{-1}, \gamma_{-1}, T_{m0}\big), \tag{22}$$

where β_{-1} and γ_{-1} define the initial (sunrise) position of the active surface, and T_{m0} is the panel initial temperature.

Considering these facts, the final optimization problem can be rewritten as:

$$J^*(\boldsymbol{\beta}, \boldsymbol{\gamma}) = \max_{\boldsymbol{\beta}, \boldsymbol{\gamma}} \mathbf{E}\Big\{ E_{netto}\big(\boldsymbol{\beta}, \boldsymbol{\gamma}, \mathbf{M}, \mathbf{G}, \mathbf{C}_0\big) \Big\}, \tag{23a}$$

$$\text{s.t.} \begin{cases} \beta_{min} \leq \boldsymbol{\beta} \leq \beta_{max}, & \boldsymbol{\beta} \in \mathbb{R}^N, \\ \gamma_{min} \leq \boldsymbol{\gamma} \leq \gamma_{max}, & \boldsymbol{\gamma} \in \mathbb{R}^N, \\ \beta_k = m_\beta \beta_q, & m_\beta \in \mathbb{Z}, \\ \gamma_k = m_\gamma \gamma_q, & m_\gamma \in \mathbb{Z}, \end{cases} \tag{23b}$$

with respect to (i) developed solar irradiance model with its uncertainty, (ii) tilted surface model, and (iii) power production and thermal model of a PV panel.

4.2. *Differential evolution*

Differential Evolution (DE) is a method that optimizes a problem solution by iteratively trying to improve a candidate solution with regard to a given measure of quality that is defined through objective function. DE's most versatile implementation maintains a pair of vector populations, both of which contain N_P D-dimensional vectors of real-valued optimization variables [10]. The current population size does not change during optimization process.

Gradient-based optimization techniques are inapplicable in the considered optimization problem because of the nature of the Unscented transformation, where posterior mean and covariance is computed based on so-called sigma points mapping instead of single point mapping. Differential evolution as one of non-gradient-based pointwise optimization techniques was chosen for several reasons: (i) easy parallelization of the algorithm and (ii) feasible optimization point can be trivially found since the constraints are imposed directly on manipulated variables.

The current population, denoted with $\mathbf{P_u}$, is composed of those vectors $\mathbf{u}_i^g$ that have already been found to be acceptable either as initial points, or by comparison with other vectors (i.e. solutions):

$$\mathbf{P}_\mathbf{u}^g = \left\{ \begin{array}{cccc} \mathbf{u}_1^g & \mathbf{u}_2^g & \dots & \mathbf{u}_{N_P}^g \end{array} \right\}, \tag{24a}$$

$$\mathbf{u}_i^g = \left[\begin{array}{cccc} u_{i,1}^g & u_{i,2}^g & \dots & u_{i,D}^g \end{array} \right], \tag{24b}$$

where index g indicates the generation to which a vector belongs. In addition, each vector in population $\mathbf{P_u}$ is assigned a population index i. In given optimization problem, candidate solutions $\mathbf{u}$ of dimension $D = 2N$ are represented with tilt and azimuth angle trajectory:

$$\mathbf{u} = \left[\begin{array}{cc} \boldsymbol{\beta}^\top & \boldsymbol{\gamma}^\top \end{array} \right]^\top, \qquad \mathbf{u} \in \mathbb{R}^{2N}. \tag{25}$$

Once initialized, DE mutates each vector of the current population creating an intermediary population $\mathbf{P_m}$ of N_P mutant vectors $\mathbf{m}_i^g$:

$$\mathbf{P}_\mathbf{m}^g = \left\{ \begin{array}{cccc} \mathbf{m}_1^g & \mathbf{m}_2^g & \dots & \mathbf{m}_{N_P}^g \end{array} \right\}, \tag{26a}$$

$$\mathbf{m}_i^g = \left[\begin{array}{cccc} m_{i,1}^g & m_{i,2}^g & \dots & m_{i,D}^g \end{array} \right]. \tag{26b}$$

For each vector from the current population, a mutant vector is generated according to:

$$\mathbf{m}_i^{g+1} = \mathbf{u}_b^g + F\left(\mathbf{u}_{r1}^g - \mathbf{u}_{r2}^g\right) = \mathbf{u}_b^g + F\Delta\mathbf{u}_{r1,2}^g, \tag{27}$$

where $\mathbf{u}_b^g$ is the best unit from the current population $\mathbf{P}_\mathbf{u}^g$, r_1 and r_2 are random integer mutually different indices with the uniform distribution on interval $[1, N_P]$, and F is the so-called spreading factor – real and constant factor from interval $[0, 1]$, which controls the amplification of the differential variation $\Delta\mathbf{u}_{r1,2}^g$. This type of mutation strategy is known as a DE/Best/1 mutation [32]. If number of current population vectors is high enough, it is possible to use two differential variations in mutation process, which can improve the diversity of the population [9].

Each vector in the current population is then recombined with its mutant to produce a trial population $\mathbf{P_c}$ of N_P trial vectors $\mathbf{c}_i^g$:

$$\mathbf{P}_\mathbf{c}^g = \left\{ \begin{array}{cccc} \mathbf{c}_1^g & \mathbf{c}_2^g & \dots & \mathbf{c}_{N_P}^g \end{array} \right\}, \tag{28a}$$

$$\mathbf{c}_i^g = \left[\begin{array}{cccc} c_{i,1}^g & c_{i,2}^g & \dots & c_{i,D}^g \end{array} \right]. \tag{28b}$$

Aforementioned vector recombination is often referred to as crossover. In literature, there are many types of crossovers [10], each suitable for certain types of optimization problems. In considered optimization problem, we use weighted arithmetic crossover:

$$\mathbf{c}_i^{g+1} = w\mathbf{u}_i^g + (1 - w)\mathbf{m}_i^{g+1}, \tag{29}$$

where w is a user-defined weighting factor from interval $[0, 1]$. During crossover trial vectors overwrite the mutant population, so a single array can hold both populations in the implementation.

The last operation in a single iteration of the DE algorithm is called selection. To decide whether or not it should become a member of next generation, the trial vector $\mathbf{c}_i^{g+1}$ is compared to the target vector $\mathbf{u}_i^g$ using the greedy criterion. If vector $\mathbf{c}_i^{g+1}$ yields a better objective function value than $\mathbf{u}_i^g$, then $\mathbf{u}_i^{g+1}$ is set to $\mathbf{c}_i^{g+1}$, otherwise the old value $\mathbf{u}_i^g$ is sustained. In the considered maximization problem, this can be formulated as:

$$\mathbf{u}_i^{g+1} = \begin{cases} \mathbf{c}_i^{g+1}, & \text{if } J(\mathbf{c}_i^{g+1}) \geq J(\mathbf{u}_i^g), \\ \mathbf{u}_i^g, & \text{otherwise}, \end{cases} \tag{30}$$

where J is the previously defined objective function (21).

Compared to gradient-based optimizers, evolutionary algorithms demand more processing capacity because they typically require more objective function evaluations. The time required to generate trial vectors is small compared to the time needed to evaluate the objective function. In real-world applications, it is not uncommon for the objective function evaluation to consume more than 95% of the total CPU time. The need for faster processing is particularly acute when optimizing objective functions evaluated via simulations, since an acceptable solution may require tens of thousands of objective function evaluations. An efficient parallel approach to such problems is crucial, since a serial processor may take hundreds of hours to optimize models based on simulations. Since

objective function evaluations for units within one generation are not mutually dependent, this task is distributed on all available processor units via a parallel computing engine, like Matlab® Parallel Computing Toolbox [33].

Evolutionary algorithms like DE are commonly known as metaheuristics as they make few or no assumptions about the problem being optimized. However, for faster convergence, we propose the following initialization method of the population $\mathbf{P}_{\mathbf{u}}^{0}$:

- 20% of the population is generated randomly with uniform distribution over the search space, with respect to the upper and lower bounds,
- 30% of the population is generated randomly within $\pm 5^{\circ}$ of the solar zenith and azimuth angle trajectory, with uniform distribution,
- 30% of the population is generated randomly within $\pm 5^{\circ}$ of the tilt and azimuth angle trajectory that instantly maximizes incoming solar irradiance,
- 20% of the population is generated randomly within $\pm 5^{\circ}$ of the optimal tilt and azimuth fixed angles on a daily basis, with uniform distribution. These optimal angles are obtained via separate DE optimization process, where all units of the current population are initialized randomly with uniform distribution over the search space.

Proposed method of the current population initialization performs coarse and fine search for an optimal solution.

A very important part of DE optimization is implementation of stopping criteria. The stopping criteria are implemented as follows [34]:

- Exhaustion-based criteria – when maximum number of generations G_{max} is reached, the optimization process is terminated. After preliminary tests, maximum number of generations is set to be $G_{max} = 500$.
- Improvement-based criteria – if there is no improvement over some predefined number of generations, the optimization process is terminated. For this purpose we compare best units of the current generation population $\mathbf{P}_{\mathbf{u}}^{g}$ and the population distanced from the current one by 25 generations $\mathbf{P}_{\mathbf{u}}^{g-25}$.
- Distribution-based criteria – for DE usually all individuals converge to the optimum eventually. Therefore, it can be concluded that convergence is reached when the individuals are close to each other. For this purpose we compare the current population's best and worst unit. If the difference between the best and the worst unit's objective function value is within 0.01 Wh, the optimization process is terminated.

Because of the implemented stopping criteria, the positioning system trajectories determined with the optimization are not guaranteed to be the best possible. In order to use the proposed procedure in applications, optimization time and computational effort have to be taken into consideration. The DE parameters and the stopping criteria are tuned in such a way to keep the computation time acceptable for the particular application.

4.3. Used model predictive control scheme

We propose an open-loop model predictive control scheme where the optimal tilt and azimuth angle trajectory is computed once a day, typically just before sunrise. The optimization considers the available local weather forecast for the entire day, with its corresponding uncertainty, and the current PV panel orientation and temperature. The optimal β and γ sequence is then transmitted to the positioning controller for daily execution. The discretization time T used in our approach is 15 min, set heuristically considering optimization process complexity and overall weather dynamics.

The other advantages of the proposed algorithm are: (i) the positioning system is controlled smoothly which reduces the positioning mechanism-outwear compared to counterpart closed-loop control systems and (ii) prediction of energy yield one day ahead is available together with its uncertainty for easier integration into the higher-level smart grid control applications.

5. Results

Developed open-loop control algorithm for dual-axes positioning system is first tested on three exemplary days with different cloudiness: (i) clear-sky, (ii) partly cloudy, and (iii) overcast. Then a year-scale comparison of developed algorithm with the open-loop solar disk tracking and the closed-loop maximum irradiance seeking algorithms is performed. All results presented in this section are given for the WDC Dulles location for the year 2005. The proposed method is general and gives the optimal results for the applied (i) solar irradiance prediction model, (ii) dynamic panel power production and thermal model, and (iii) the positioning system energy consumption model with its technical constraints. Generality of the proposed method remains even in the case when the applied models are replaced with the more detailed ones.

5.1. Simulation scenario

We consider 15 poly-Si PV panels SV60–235 (single panel power rating: $235\,\mathrm{Wp}$) manufactured by Solvis Ltd. with overall active surface area of $A = 24.895\,\mathrm{m}^2$, with the dual-axes positioning system described in [6, 7]. The explained procedure is verified on three exemplary days with different cloudiness: (i) clear-sky, (ii) partly cloudy, and (iii) overcast weather conditions. Simulation scenarios for considered exemplary days are shown in Figure 5, where referenced figure shows expected profile of the direct (normal) and diffuse (horizontal) solar irradiance.

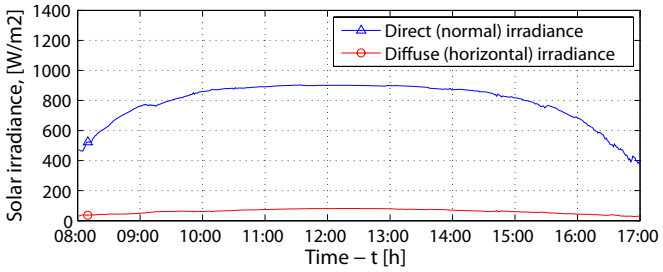

(a) Expectation of solar irradiance components for the clear-sky day

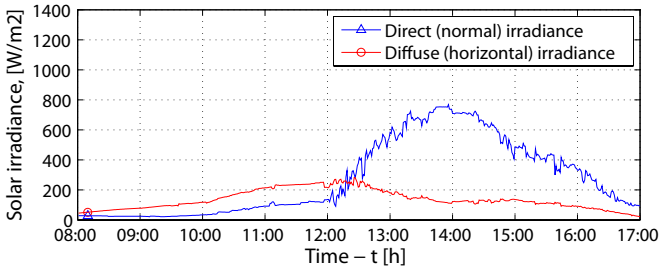

(b) Expectation of solar irradiance components for the partly cloudy day

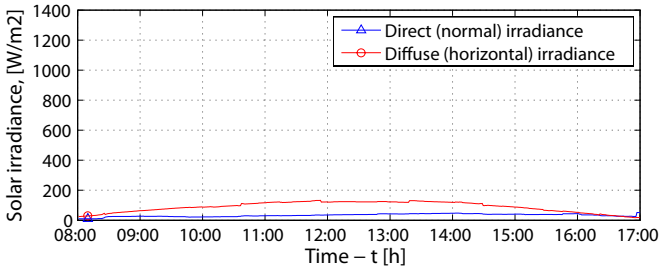

(c) Expectation of solar irradiance components for the overcast day

Figure 5: Expected profile of the direct (normal) and diffuse (horizontal) solar irradiance components for considered three exemplary days

All input meteorological data are assumed to be subject to a Gaussian uncertainty, where data variance is given in a form of percentage points of the data expected value. In some cases variance is held at constant value, while in other cases it linearly increases during the day from 0% to some final value: (i) aerosol optical thickness and precipitable water vapor thickness is with constant variance of 5% during the day, (ii) total and opaque cloud cover variance linearly increases with an end-day variance of 20%, (iii) dry-bulb temperature variance linearly increases with an end-day variance of 10%, and (iv) local air pressure variance linearly increases with an end-day variance of 0.5%. The input geographical and time data, i.e. the instantaneous zenith angle is assumed to have 0% variance.

During clear-sky conditions when direct irradiance prevails, optimal trajectory is the one tracking the solar disk. In this way, angle between the sun direction and the active surface normal is always $\theta = 0°$, and according to (9) direct irradiance component is best harvested. During overcast conditions when diffuse irradiance prevails, optimal trajectory would be the fixed active surface, with the tilt angle $\beta = 0°$. In this way most of the diffuse irradiance component is being harvested, since diffuse irradiance is scattered all over the sky. For clear-sky and overcast conditions optimal trajectory is well known. However, during partly cloudy conditions when neither direct or diffuse component is dominant, optimal trajectory makes a compromise between harvesting direct and diffuse solar irradiance components.

5.2. *The considered positioning system*

The positioning system must be described with a proper model in order to be included in the optimization procedure. It must be noted that the complexity of the applied model can substantially increase the required computational effort and consequently the time required for optimization. In this paper, the positioning system energy consumption model is given in the form of the angle-change-dependent characteristics [6]. Angle-change-dependent energy consumption characteristics of the considered positioning system are shown in Figure 6.

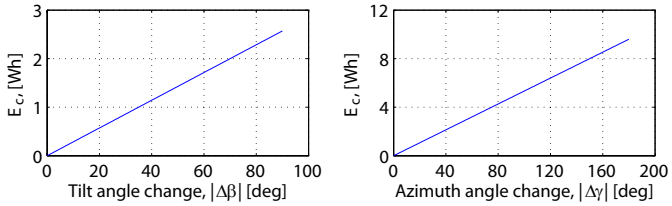

Figure 6: The positioning system energy consumption characteristics [6]

The considered positioning system (i) minimum and maximum allowed surface tilt and azimuth angles, β_{min}, β_{max}, γ_{min} and γ_{max} are $0°$, $85°$, $75°$, and $285°$, respectively, and (ii) resolution quants, β_q and γ_q, are $0.01°$.

5.3. *Optimal trajectories on three exemplary days*

Optimization process begins with prediction of expected solar irradiance on the prediction horizon of one day based on the developed site-specific solar irradiance models as described in Section 2. Uncertainty of the developed irradiance model is also taken into account in a form of a standard deviation around expected solar irradiance. Up to this step, calculation does not depend on the PV panel's active surface tilt and azimuth angles. However, to calculate solar irradiance incident with a tilted surface and later power production profile, tilt and azimuth angles of the active surface must be known. As tilt and azimuth angles over prediction horizon are represented via DE's candidate solution $\mathbf{u}_i^g$, this step is performed repeatedly in each candidate solution evaluation.

In DE optimization algorithm evaluation procedure, three different types of the dual-axes positioning system trajectories for tilt and azimuth angles are compared: (i) optimal trajectory obtained by DE optimization as described in Section 4, denoted with OPT, (ii) solar disk tracking by its zenith and azimuth angles, denoted with SUN, and (iii) tilt and azimuth angle trajectory that instantly maximizes incoming solar irradiance regardless

to the positioning system energy consumption, denoted with REC. Aforementioned trajectories are evaluated by calculating netto energy production gain of the PV system in a stochastic framework, for each exemplary day. Numerical results of the PV panel netto energy production over the whole exemplary day for different trajectories are shown in Table 2. As it can be seen, greatest improvement of optimal trajectory compared to solar disk tracking is during partly cloudy and overcast conditions, while compared to trajectory for instantaneous maximization of incoming solar irradiance that is the case during partly cloudy conditions.

Table 2: The PV system netto energy production (Wh)

	Optimal traj. OPT	Sun tracking SUN	Max. irrad. REC
Clear-sky	28322	28303	28305
Partly cloudy	12754	12602	12736
Overcast	3461	3273	3457

OPT – Optimal trajectory obtained by DE, SUN – Solar disc tracking, REC – Trajectory for instantly maximiz. of incoming solar irradiance

Figure 7 and Figure 8 show (i) optimal trajectory obtained by DE optimization, (ii) solar disk zenith and azimuth angles, and (iii) optimal daily PV panel fixed angles. In Figure 7 uncertainty of the input meteorological data and of the developed solar irradiance models is neglected, while it is included in Figure 8.

During clear-sky condition optimal trajectory follows the sky position of the solar disk in order to maximize direct solar irradiance harvesting. Note that there is no major difference between optimal clear-sky trajectories in deterministic and stochastic framework, since probability for sudden change in cloudiness is minimal. During overcast condition in deterministic framework, PV panel is in rest since it is not profitable to reposition in order to harvest minimal portion of direct irradiance, while in stochastic framework where there exists probability of higher portion of direct irradiance, PV panel repositions but still on low tilt angles in order to harvest most of the available diffuse solar irradiance. During partly cloudy condition, PV panel stays on low tilt angles when diffuse irradiance prevails, and follows the sky position of the solar disk when direct irradiance prevails. In the stochastic environment during cloudy part of the day, tilt angle is larger compared to the deterministic environment due to accounted gain of possible increase in direct irradiance.

5.4. Tuning DE strategy parameters

In model predictive control, optimization time and computational effort can be an aggravating circumstance for its practical use. Besides the complexity of the model involved, strategy parameters used within DE optimization algorithm also significantly affect optimization time. DE algorithm is implemented with support of Matlab® Parallel Computing Toolbox [33], using all available processor units. Optimization is performed on the following computer configuration:

```
Intel(R) Core(TM)2 Quad CPU,
Q8300 @ 2.50GHz 2.50GHz,
4,00 GB of RAM (3,44 GB usable),
```

where optimization time for each day is estimated to be nearly 12 min in average. DE optimization strategy parameters are tuned via trial–error method, considering quality of found solution and optimization time.

5.5. Algorithms comparison on a year-scale

In order to get more realistic picture about the improvement that the proposed predictive control offers, its evaluation is performed on a year-scale. Performance comparison of dual-axes positioning system with single-axis or no positioning is already well known [35, 36], and here we focus on comparison between the proposed and most commonly used dual-axes positioning algorithms. Input meteorological and geographical data are taken from NSRDB for the year 2005. Evaluation scenario consists of 100 different direct (normal) and diffuse (horizontal) irradiance components profiles, that are generated via random number generator with Gaussian distribution, with respect to expectation and variance of irradiance components at full hour. Minute resolution of solar irradiance components is obtained by linear interpolation between full hour samples. Daily netto energy production is calculated as a mean value of all 100 daily scenarios.

Figure 9 shows (i) overall monthly insolation per unit area, (ii) average monthly temperature for sunlight period, and (iii) overall monthly netto electrical energy production of the considered PV system using three different types of trajectories: (iii-a) optimal trajectory obtained by DE optimization, (iii-b) solar disk tracking by its zenith and azimuth angles, and (iii-c) tilt and azimuth angle trajectory that instantly maximizes incoming solar irradiance regardless to the positioning system energy consumption. Tilt and azimuth angle trajectory that instantly maximizes incoming solar irradiance is calculated and evaluated individually for each of the 100 daily scenarios.

On the year-basis optimal trajectories obtained by DE optimization give 0.37% increased power production compared to the solar disk sky position tracking, and 1.27% increased power production compared to the trajectory that instantly maximizes incoming solar irradiance. The proposed control of orientation of the active surface gives better results than state-of-the-art solutions, and on the large scale it can lead to a substantial economic gain. The proposed approach does not require additional sensors, acts smoothly on the individual axes positioning system (taking the whole day into account for the positioning decision), and provides the expected power production together with its variance as data ready for incorporation in higher-level smart grid control applications [37, 38, 39].

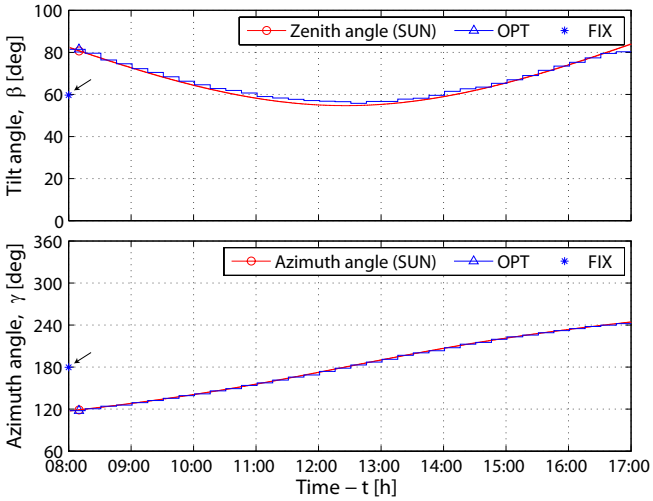

(a) Tilt and azimuth angle trajectories for the clear-sky day

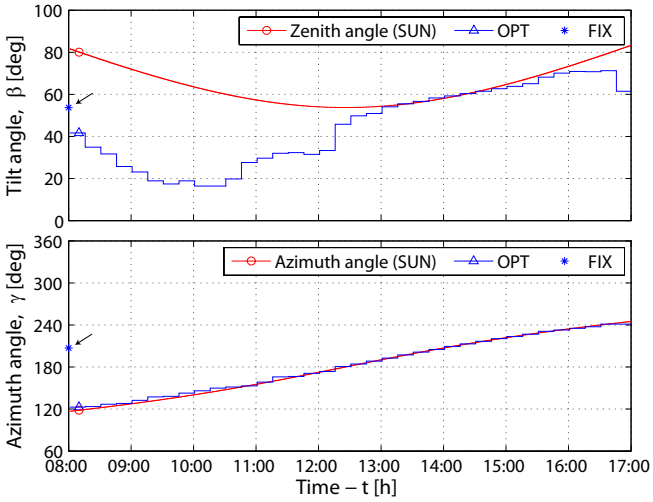

(b) Tilt and azimuth angle trajectories for the partly cloudy day

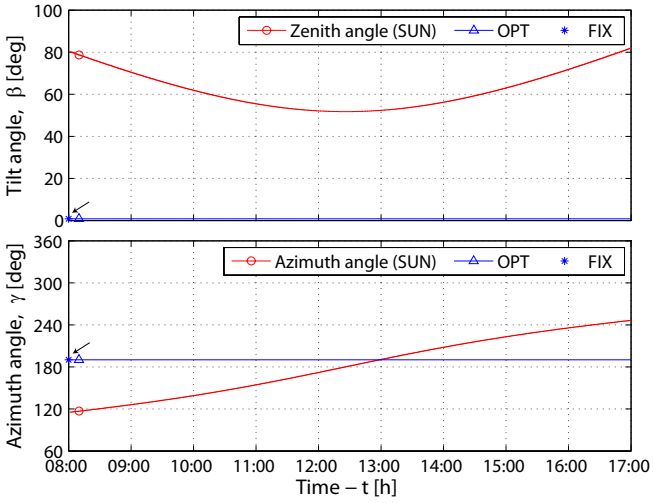

(c) Tilt and azimuth angle trajectories for the overcast day

Figure 7: Tilt and azimuth angle trajectories of the PV panel positioning system in a deterministic framework for considered exemplary days

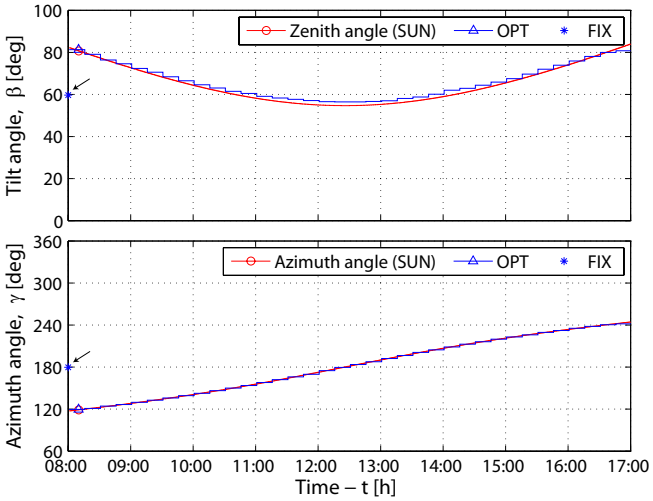

(a) Tilt and azimuth angle trajectories for the clear-sky day

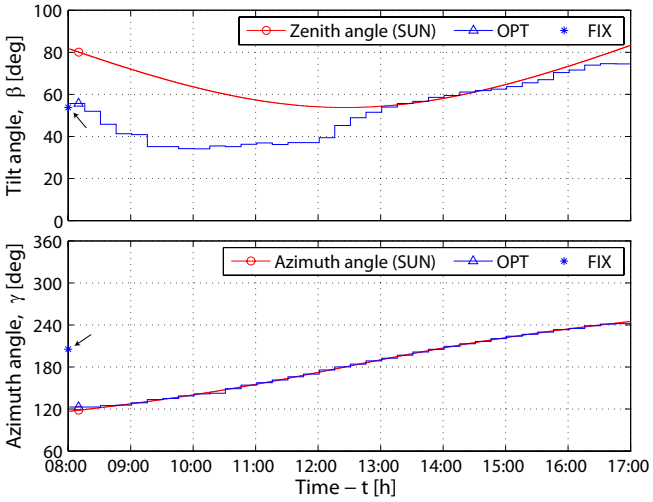

(b) Tilt and azimuth angle trajectories for the partly cloudy day

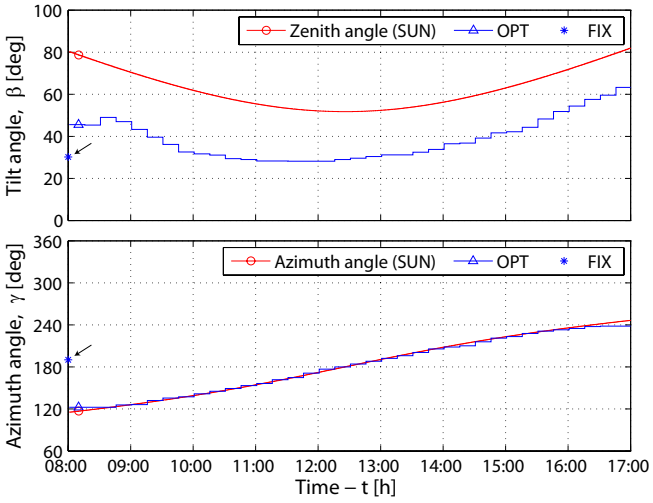

(c) Tilt and azimuth angle trajectories for the overcast day

Figure 8: Tilt and azimuth angle trajectories of the PV panel positioning system in a stochastic framework for considered exemplary days

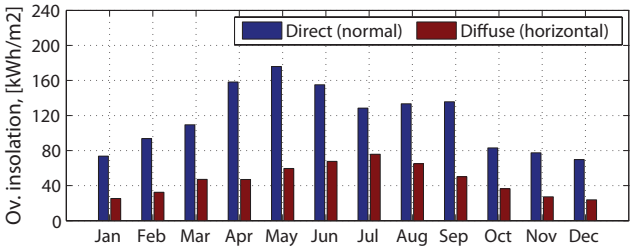

(a) Overall monthly solar insolation per unit area

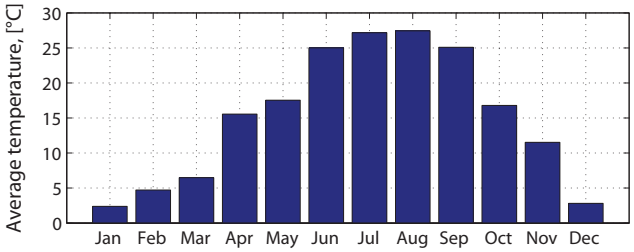

(b) Average monthly temperature for sunlight period

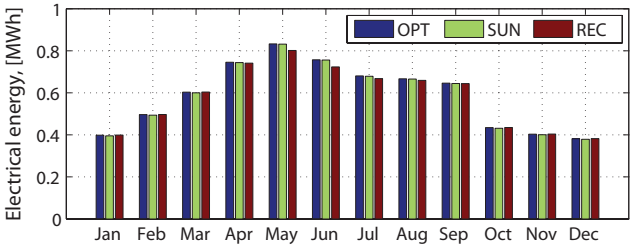

(c) Overall monthly netto electrical energy production

Figure 9: Results of the year-scale evaluation for WDC Dulles

6. Conclusion

In this paper a model predictive control algorithm for dual-axes positioning system of a photovoltaic system is described. The model predictive control synthesis procedure comprises two basic steps: (i) identification of solar irradiance model and development of the photovoltaic system model and (ii) development of predictive control algorithm of photovoltaic panel orientation based on the obtained models. The proposed method is general and accounts for: (i) local weather forecast and its uncertainty, (ii) solar irradiance model and its uncertainty, (iii) dynamic panel power production and thermal model, and (iv) positioning system energy consumption with its technical constraints. Generality of the proposed method remains even in the case when the applied models are replaced with the more detailed ones. Developed method for determining maximum efficiency trajectories shows increased power production in all operating environments, compared to the state-of-the-art dual-axes positioning solutions. The proposed approach does not require additional sensors, acts smoothly on the positioning system, and provides the expected power production with its variance as data ready for incorporation in higher-level smart grid control applications.

Acknowledgments

This work has been financially supported by Croatian Science Foundation under grant No. I-4463-2011 (MICROGRID) and by the European Community Seventh Framework Programme under grant No. 285939 (ACROSS). This support is gratefully acknowledged.

References

[1] REN21 Renewable Energy Policy Network, Renewables 2010: Global Status Report, REN21 Secretariat, Paris, 2010.
[2] German Advisory Council on Global Change, World in Transition: A Social Contract for Sustainability (2011).
[3] K. S. Karimov, M. A. Saqib, P. Akhter, M. M. Ahmed, J. A. Chattha, S. A. Yousafzai, A simple photo-voltaic tracking system, Solar Energy Materials & Solar Cells 87 (1) (2005) 49–59.
[4] R. Ranganathan, W. Mikhael, N. Kutkut, I. Batarseh, Adaptive sun tracking algorithm for incident energy maximization and efficiency improvement of pv panels, Renewable Energy 36 (10) (2011) 2623–2626.
[5] H. Mousazadeh, A. Keyhani, A. Javadi, H. Mobli, K. Abrinia, A. Sharifi, A review of principle and sun-tracking methods for maximizing solar systems output, Renewable and Sustainable Energy Reviews 13 (8) (2009) 1800–1818.
[6] S. Seme, G. Štumberger, J. Voršič, Maximum efficiency trajectories of a two-axis sun tracking system determined considering tracking system consumption, Power Electronics, IEEE Transactions on 25 (4) (2011) 1280–1290.
[7] S. Seme, G. Šturmberger, A novel prediction algorithm for solar angles using solar radiation and differential evolution for dual-axis sun tracking purposes, Solar Energy 85 (11) (2011) 2757–2770.
[8] N. A. Kelly, T. L. Gibson, Improved photovoltaic energy output for cloudy conditions with a solar tracking system, Solar Energy 83 (11) (2009) 2092–2102.
[9] R. Storn, K. Price, Differential evolution – a simple and efficient heuristic for global optimization over continuous spaces, Journal of Global Optimization 11 (4) (1997) 341–359.
[10] K. V. Price, R. M. Storn, J. A. Lampinen, Differential Evolution: A Practical Approach to Global Optimization, Springer-Verlag, 2005.
[11] L. T. Wong, W. K. Chow, Solar radiation model, Applied Energy 69 (3) (2001) 191–224.
[12] A. S. S. Dorvlo, J. A. Jervase, A. Al-Lawati, Solar radiation estimation using artificial neural networks, Applied Energy 71 (4) (2002) 307–319.
[13] G. Reikard, Predicting solar radiation at high resolutions: A comparison of time series forecasts, Solar Energy 83 (3) (2009) 342–349.
[14] S. Janjai, K. Sricharoen, S. Pattarapanitchai, Semi-empirical models for the estimation of clear sky solar global and direct normal irradiances in the tropics, Applied Energy 88 (12) (2011) 4749–4755.
[15] A. Mellit, H. Eleuch, M. Benghanem, C. Elaoun, A. M. Pavan, An adaptive model for predicting of global, direct and diffuse hourly solar irradiance, Energy Conversion and Management 51 (4) (2010) 771–782.
[16] S. Wilcox, National Solar Radiation Database 1991–2005 Update: User's Manual, Tech. rep., National Renewable Energy Laboratory (2007).
[17] I. Reda, A. Andreas, Solar position algorithm for solar radiation applications, Tech. rep., National Renewable Energy Laboratory (2008).
[18] M. Vašak, M. Gulin, J. Čeović, D. Nikolić, T. Pavlović, N. Perić, Meteorological and weather forecast data-based prediction of electrical power delivery of a photovoltaic panel in a stochastic framework, in: MIPRO, 2011 Proceedings of the 34th International Convention on Information and Communication Technology, Electronics and Microelectronics, Opatija, Croatia, 2011, pp. 733–738.
[19] E. L. Maxwell, Metstat – the solar radiation model used in the production of the national solar radiation data base (nsrdb), Solar Energy 62 (4) (1998) 263–279.

[20] B. G. Kermani, S. S. Schiffman, H. T. Nagle, Performance of the levenberg-marquardt neural network training method in electronic noise applications, Sensors and Actuators B: Chemical 110 (1) (2005) 13–22.
[21] R. C. Green, L. Wang, M. Alam, Training neural networks using central force optimization and particle swarm optimization: Insights and comparisons, Expert Systems with Applications 39 (1) (2012) 555–563.
[22] S. Kiranyaz, T. Ince, A. Yildirim, M. Gabbouj, Evolutionary artificial neural networks by multi-dimensional particle swarm optimization, Neural Networks 22 (10) (2009) 1448–1462.
[23] S. Chen, B. Mulgrew, P. M. Grant, A clustering technique for digital communications channel equalization using radial basis function networks, Neural Networks, IEEE Transactions on 4 (4) (1993) 570–590.
[24] A. A. El-Sebaii, F. S. Al-Hazmi, A. A. Al-Ghamdi, S. J. Yaghmour, Global, direct and diffuse solar radiation on horizontal and tilted surfaces in jessah, saudi arabia, Applied Energy 87 (2) (2010) 568–576.
[25] A. Padovan, D. Del Col, Measurement and modeling of solar irradiance components on horizontal and tilted planes, Solar Energy 84 (12) (2010) 2068–2084.
[26] C. K. Pandey, A. K. Katiyar, A note on diffuse solar radiation on a tilted surface, Energy 34 (11) (2009) 1764–1769.
[27] S. A. Barakat, Comparison of models for calculating solar radiation on tilted surfaces, in: Proceedings of the 4th International Symposium on the Use of Computers for Environmental Engineering Related to Buildings, Tokyo, Japan, 1983, pp. 317–322.
[28] J. Twidell, T. Weir, Renewable Energy Resources, Taylor & Francis, 2006.
[29] E. A. Wan, R. van der Merwe, The unscented kalman filter, in: Kalman Filtering and Neural Networks, John Wiley & Sons, 2001.
[30] A. D. Jones, C. P. Underwood, A thermal model for photovoltaic systems, Solar Energy 70 (4) (2001) 349–359.
[31] S. Armstrong, W. G. Hurley, A thermal model for photovoltaic panels under varying atmospheric conditions, Applied Thermal Engineering 30 (11) (2010) 1488–1495.
[32] R. Mallipeddi, P. N. Suganthan, Q. K. Pan, M. F. Tasgetiren, Differential evolution algorithm with ensemble of parameters and mutation strategies, Applied Soft Computing 11 (2) (2011) 1679–1696.
[33] The MathWorks, Inc., Parallel Computing Toolbox^{TM}.
[34] K. Zielinski, P. Weitkemper, R. Laur, K. D. Kammeyer, Examination of stopping criteria for differential evolution based on a power allocation problem, in: 10th International Conference on Optimization of Electrical and Electronic Equipment, Brasov, Romania, 2006, pp. 149–156.
[35] T. Maatallah, S. E. Alimi, S. B. Nassrallah, Performance modeling and investigation of fixed, single and dual-axis tracking photovoltaic panel in monastir city, tunisia, Renewable and Sustainable Energy Reviews 15 (8) (2011) 4053–4066.
[36] T. P. Chang, Output energy of a photovoltaic module mounted on a single-axis tracking system, Applied Energy 86 (10) (2009) 2071–2078.
[37] M. Chaabene, M. B. Ammar, A. Elhajjaji, Fuzzy approach for optimal energy-management of a domestic photovoltaic panel, Applied Energy 84 (10) (2007) 992–1001.
[38] Y. Su, L.-C. Chan, L. Shu, K.-L. Tsui, Real-time prediction models for output power and efficiency of grid-connected solar photovoltaic systems, Applied Energy 93 (2012) 319–326.
[39] M. B. Ammar, M. Chaabene, A. Elhajjaji, Daily energy planning of a household photovoltaic panel, Applied Energy 87 (7) (2010) 2340–2351.